Influence of finite spatial resolution on single- and double-pass femtosecond pulse shapers

Franziska Frei,* Reto Bloch, and Thomas Feurer

Institute of Applied Physics, University of Bern, Sidlerstrasse 5, CH-3012 Bern, Switzerland
**Corresponding author: franziska.frei@iap.unibe.ch*

Received August 23, 2010; revised November 3, 2010; accepted November 5, 2010;
posted November 5, 2010 (Doc. ID 133766); published November 30, 2010

We investigate the influence of the finite spatial resolution of a typical $4f$ pulse-shaping setup in a single- and double-pass configuration on the shaped waveforms. Specifically, we calculate and measure the space-frequency distribution at the focal plane of a lens following the shaping setup and show that steep amplitude or phase jumps, as they appear with pixelated spatial light modulators, are affected by a finite spatial resolution.

OCIS codes: 320.0320, 320.5540.

Tailored ultrashort laser pulses find applications in a variety of fundamental, as well as applied, sciences [1]. They are a powerful tool for nonlinear spectroscopy [2], nonlinear microscopy [3], selective femtochemistry [4], and coherent control [5]. Over the past decades, a number of different techniques have been developed up to the point were basically all degrees of freedom of an ultrashort laser pulse can be manipulated, i.e., spectral amplitude, phase, and polarization. Most experiments use a spatial light modulator (SLM) in the symmetry plane of a $4f$ zero-dispersion compressor; these SLMs may be pixelated or nonpixelated, depending on the nature of the device. In many cases, it is important to have a detailed theoretical model of the waveform produced. A first Fourier optical model of a $4f$ pulse-shaping setup was reported by Wefers and Nelson [6]. It explained many features of pulse shaping; specifically, it showed that temporal shaping comes at the expense of spatial shaping—a phenomenon that is known as space–time coupling. These effects, and especially their influence on experiments, were further analyzed by other groups [7–9]. While space–time coupling appears for all types of SLMs, pixelated devices introduce additional complications that lead to the appearance of waveform replicas; their origin and their properties were thoroughly analyzed in [10]. Here, we investigate theoretically as well as experimentally the influence of finite spatial resolution on the waveforms produced. Specifically, we analyze a $4f$ setup in single- and double-pass geometry [6].

We start by analyzing the effects of finite spatial resolution based on Fourier optical simulations, and we show experimental results that verify the theoretical findings. Specifically, we investigate the space-frequency distribution of shaped waveforms at the focal plane of a focusing lens (f_2) after the pulse shaper. We use scalar fields, the transfer functions for free-space propagation, a lens in paraxial approximation, and the transfer function of a grating or a prism with linearized angular dispersion. A one-dimensional treatment suffices, as the vertical electric-field component remains unaffected by the pulse shaper. With these we find for the space-frequency distribution:

$$\mathcal{E}(x,\Omega) \propto \mathcal{E}_0\left(-\frac{k_c}{f_2}x,\Omega\right) M\left(\frac{f\gamma}{k_c}\Omega + \frac{fb}{f_2}x\right). \tag{1}$$

The spectral field $\mathcal{E}_0(x,\Omega)$ is the one-time Fourier transform of the slowly varying envelope $\mathcal{E}_0(x,t)$ of the incident pulse, $\Omega = \omega - \omega_c$ is the relative frequency with respect to the carrier frequency ω_c, and k_c is the wave vector at ω_c. The pulse-shaping setup is described by the focal length f, $b = \cos\alpha/\cos\beta_c$, $\gamma = 2\pi m/(\omega_c G \cos\beta_c)$, the diffraction order m, the angle of incidence on the first grating α, the diffraction angle β_c at ω_c, and the grating constant G. The SLM transfer function is $M(x)$. Equation (1) describes pulse shaping sufficiently accurately for most purposes. Specifically, it includes space–time coupling effects and waveform replicas when the SLM transfer function $M(x)$ is pixelated. Space–time coupling is quantified through

$$x = -\frac{f\gamma}{k_c}\Omega. \tag{2}$$

Equation (1) is derived under the assumption of ideal lenses, i.e., lenses with an infinitely large aperture and no aberrations and thus neglects all effects due to finite spatial resolution. To include finite resolution, we convolute the field in Eq. (1) with the point-spread function $P(x)$:

$$\mathcal{E}_1(x,\Omega) = \int \mathrm{d}x' P(x')\mathcal{E}(x-x',\Omega). \tag{3}$$

We expect that the finite resolution becomes important if either the amplitude modulation or the phase modulation applied are on similar length scales as $P(x)$. Pixelated SLMs should be particularly susceptible because all transitions between two neighboring pixels are potentially steeper than the width of $P(x)$. For example, steep amplitude modulations appear whenever the spectral transmission drops from one to zero from one pixel to the next; steep phase jumps occur when the phase function applied has to be wrapped because of a limited accessible phase range (typically a little more than 2π). For these reasons, we will examine two cases, namely setting the transmission of a single pixel to zero and, second,

introducing an abrupt phase jump with an amplitude between 0 and 2π to an otherwise flat phase.

The experiments are performed with a Ti:sapphire oscillator emitting 60 nm broad pulses at a center wavelength of 820 nm and a repetition rate of 90 MHz. The pulse shaper consists of a $4f$ zero-dispersion compressor equipped with a 640 pixel SLM (JenOptik SLM 640-d); details can be found in [9]. The waveforms exiting the pulse shaper are focused by a lens with a focal length of 400 mm in $2f$ geometry. The relevant $P(x)$ is from the position of the SLM to the focal plane of the last lens. It is calculated with ZEMAX, is approximately Gaussian in shape, has a FWHM of 35 μm, and agrees reasonably well with the experimental value of (40 ± 3) μm. The space-frequency intensity distribution at the focal plane $I(x, \Omega)$ is analyzed with a high-resolution imaging spectrometer equipped with a CCD camera. Its spatial resolution is calculated to 23 μm and measured to (30 ± 3) μm; its spectral resolution is measured to 0.1 nm. For all simulations presented hereafter, we use the experimentally determined values. Additionally, we assume that the incident field $\mathcal{E}_0(x, \Omega)$ has a Gaussian spectral as well as a spatial profile.

The first $M(x)$ analyzed is the transmission of a single pixel set to zero. Figure 1(a) shows a small fraction (≈2 nm) of the measured space-frequency distribution. The amplitude drops to zero in a frequency range that corresponds to that of a single pixel, and the rising as well as the falling edges are somewhat washed out due to the finite point spread function. Moreover, the exact position of the spectral bandstop filter depends on the spatial coordinate x, which is a consequence of space–time coupling. The dashed–dotted lines indicate space–time coupling according to Eq. (2). In all aspects, the measured results correspond well to the simulations in Fig. 1(b).

While the influence of finite resolution on amplitude modulations bears little surprises, the situation is somewhat less obvious for steep phase jumps. We begin our discussion with an often-used π phase step. Figure 1(c) shows the measured space-frequency intensity distribution when a π phase step is applied from one pixel to the next. Surprisingly, an amplitude modulation appears, and its width is smaller than the width of a single pixel. Inspection of Eq. (1) reveals that without finite spatial resolution, a pure phase modulation should have no influence on the spectral intensity. With finite resolution, the situation is different and Eq. (3) predicts an amplitude modulation, as shown in Fig. 1(d), which agrees well with the experimental result. While the tilt is a consequence of space–time coupling, the width is dominated by the width of $P(x)$. One may argue that the electric field at a specific frequency is a coherent superposition of the entire spatial support of $P(x)$ at the plane of the SLM. That is, if a π phase step is applied, then one-half of $P(x)$ will experience no phase modulation, while the other half will be π phase shifted; the two halves will interfere destructively, and the intensity at this frequency will be zero. In case the phase step applied is somewhat washed out, the intensity does not drop all the way to zero and the remaining intensity bears some information on the shape of the phase step itself.

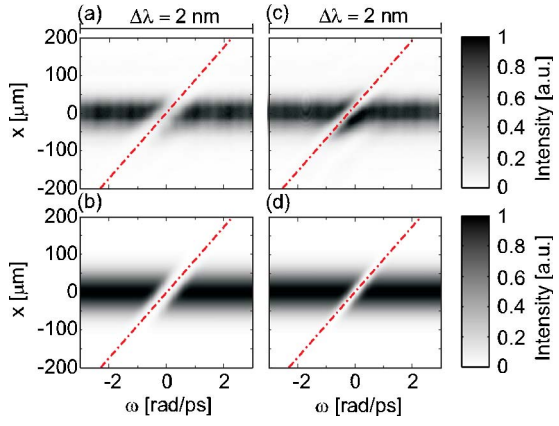

Fig. 1. (Color online) Space-frequency intensity distribution for the transmission of a single pixel set to zero—(a) experiment and (b) simulation—and for a π phase jump between two neighboring pixels—(c) experiment and (d) simulation. The dashed–dotted lines correspond to space–time coupling as predicted by Eq. (2).

The intensity plot in Fig. 2 shows the spectral intensity at $x = 0$ as a function of frequency and the amplitude of the phase step ranging from 0 to 2π. A comparison of the experimental results in Fig. 2(a) with the simulations in Fig. 2(b) reveals that the experimental trace is slightly asymmetric with respect to a horizontal line at a phase of π. As the amplitude of the phase step approaches 2π, the intensity modulation becomes broader and more pronounced, as predicted by the simulations, and even for 2π we observe a small spectral intensity modulation. We found that this is due to the fact that the phase step itself is not infinitely steep but has a finite slope. An important consequence of this is that all phase modulations that are smooth compared to $P(x)$ may nevertheless cause spectral modulations if phase wrapping is used.

Space–time coupling, as seen in Fig. 1, may cause problems in experiments because the response of the system investigated depends on its spatial position within the focal volume. The finite resolution of the shaping setup may cause additional complications, as discussed above. The question arises whether passing the pulse shaper a second time in the reverse direction may help to resolve some of these issues, as is the case for standard grating or prism compressors. Experimentally, we realize a double-pass configuration by a mirror directly after the second grating, sending the pulse back through the entire setup and separating it from the incident beam by a beam splitter. In the simulations we use two point-spread functions. While the first, i.e., $P_1(x)$ with a FWHM of 11 μm, accounts for the distance from the SLM to the backreflector and back to the SLM, the second, i.e., $P_2(x)$ with a FWHM of 28 μm, relates to the distance from the SLM to the

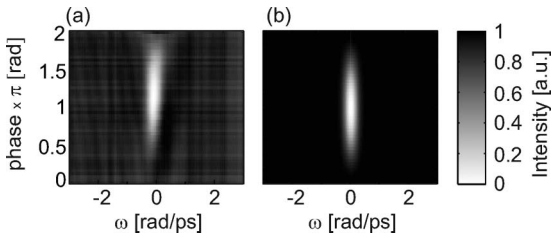

Fig. 2. (a) Measured and (b) simulated on-axis spectra ($x = 0$) at the focal plane as a function of the phase step amplitude.

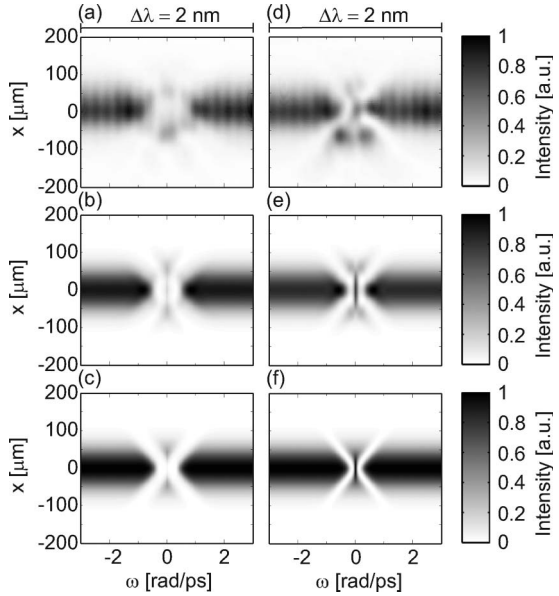

Fig. 3. Space-frequency intensity distribution for the double-pass configuration. Left column, transmission of a single pixel set to zero. Right column, π phase step. (a), (d) Experiments. Simulations (b), (e) with and (c), (f) without a second-order spatial phase.

focal plane. Similar to [6], we find for the double-pass configuration

$$\mathcal{E}_2(x,\Omega) \propto \int \mathrm{d}x'' P_2(x'') M\left(\frac{f\gamma}{k_c}\Omega + \frac{fb}{f_2}(x-x'')\right) \times \int \mathrm{d}x' P_1(x') \mathcal{E}_0\left(\frac{k_c}{bf}x' + \frac{k_c}{f_2}(x-x''),\Omega\right) \times M\left(\frac{f\gamma}{k_c}\Omega - x' - \frac{fb}{f_2}(x-x'')\right). \quad (4)$$

If we assume perfect resolution, i.e., $P_1(x) = P_2(x) = \delta(x)$, it is easy to see that space–time coupling of the second path has the opposite sign as that of the first pass. That is, space–time coupling is not canceled but appears twice with opposite signs, as can be seen in Fig. 3(c) where we again have set the transmission of a single pixel to zero. Comparing the simulations in Fig. 3(c) to the experiments in Fig. 3(a) reveals several minor discrepancies. We found that they are due to the finite propagation distance between the second grating and the backreflector as the pulse acquires a quadratic spatial phase on the order of 1.6 rad at $x = \pm 4$ mm. Although small, this additional phase alters the space-frequency intensity distribution, as seen in Fig. 3(b). The same signature is found for a π phase step, as shown in Figs. 3(d)–3(f). Here, the intensity modulation due to the finite resolution appears twice and space–time coupling causes those two modulations to have opposite slopes.

In conclusion, we demonstrated that the finite resolution of a typical $4f$ pulse shaping setup has a measurable influence on the waveforms produced. This influence is negligible for smooth amplitude or phase modulations but is detectable as soon as the modulations appear on similar length scales as the point-spread function of the shaping setup. The consequences are especially dramatic for steep phase variations as they appear for phase step modulations or phase wraps; here, a phase modulation is converted to an amplitude modulation. Finally, we confirmed experimentally that double passing the $4f$ setup does not cancel space–time coupling except for special cases, such as, for example, a linear phase modulation.

This work was supported by the National Centre of Competence in Research—Molecular Ultrafast Sciences and Technology, the research instrument of the Swiss National Science Foundation (SNSF), and SNFS grant 200020_126553/1.

References

1. A. M. Weiner, Rev. Sci. Instrum. **71**, 1929 (2000).
2. Y. Silberberg, Annu. Rev. Phys. Chem. **60**, 277 (2009).
3. P. Schön, M. Behrndt, D. Aït-Belkacem, H. Rigneault, and S. Brasselet, Phys. Rev. A **81**, 013809 (2010).
4. W. Lozovoy, X. Zhu, T. C. Gunaratne, D. A. Harris, J. C. Shane, and M. Dantus, J. Phys. Chem. A **112**, 3789 (2008).
5. D. Goswami, Phys. Rep. **374**, 385 (2003).
6. M. M. Wefers and K. A. Nelson, IEEE J. Quantum Electron. **32**, 161 (1996).
7. T. Tanabe, H. Tanabe, Y. Teramura, and F. Kannari, J. Opt. Soc. Am. B **19**, 2795 (2002).
8. B. J. Sussman, R. Lusten, and A. Stolow, Phys. Rev. A **77**, 043416 (2008).
9. F. Frei, A. Galler, and T. Feurer, J. Chem. Phys. **130**, 034302 (2009).
10. J. C. Vaughan, T. Feurer, K. W. Stone, and K. A. Nelson, Opt. Express **14**, 1314 (2006).